

## Automatic Designation of the Melting Layer with a Polarimetric Prototype of the WSR-88D Radar

SCOTT E. GIANGRANDE, JOHN M. KRAUSE, AND ALEXANDER V. RYZHKOV

*Cooperative Institute for Mesoscale Meteorological Studies, University of Oklahoma, and NOAA/OAR/National Severe Storms Laboratory, Norman, Oklahoma*

(Manuscript received 31 October 2006, in final form 3 July 2007)

### ABSTRACT

A new polarimetric melting layer detection algorithm (MLDA) is utilized to estimate the top (melting level) and bottom boundaries of the melting layer and is tailored for operational deployment. Melting layer designations from a polarimetric prototype of the Weather Surveillance Radar-1988 Doppler (WSR-88D) in central Oklahoma are validated using radiosonde and model temperature analysis. It is demonstrated that the MLDA estimates the top of the melting layer with a root-mean-square error of about 200 m within 60 km of the radar. There is evidence that the polarimetric radar might yield better spatial and temporal designation of the melting layer within the storm than that obtained from existing numerical model output and soundings.

### 1. Introduction

Accurate melting layer (ML herein) designation is useful for several operational radar applications. ML identification is needed for accurate quantitative precipitation estimation (QPE) because mixed-phase and frozen hydrometeors may contaminate radar rainfall estimates at longer distances from the radar. Knowledge of ML location is also important for microphysical characterization of the cloud, including the separation of liquid from frozen hydrometeors and evaluation of icing potential.

Melting hydrometeors often produce a discernable signature in conventional radar reflectivity factor  $Z$  known as the radar “bright band.” Gourley and Calvert (2003) describe an operational technique for brightband detection that scans columns of  $Z$  for spatially consistent maxima. The technique is recommended for stratiform precipitation events in which brightband signatures are often well pronounced and associated with melting snow aggregates. However, the transition between frozen and liquid hydrometeors in convective regions featuring melting graupel or hail is not well marked with a pronounced  $Z$  signature. The lack of

pronounced signatures is a significant challenge to conventional radar-based ML designation in convective situations.

Polarimetric radar provides a unique capability to delineate the ML. Polarimetric measurements including the differential reflectivity  $Z_{DR}$ , cross-correlation coefficient  $\rho_{HV}$ , specific differential phase  $K_{DP}$ , and linear depolarization ratio  $L_{DR}$  exhibit well-pronounced ML signatures both in stratiform and convective situations (e.g., Zrnić et al. 1993). Moreover, polarimetric measurements are sensitive to melting hydrometeors in situations where  $Z$  alone does not exhibit brightband signatures. It is known that the ML in stratiform clouds is characterized by a drop in  $\rho_{HV}$  and peaks in  $Z_{DR}$  and  $L_{DR}$  measurements. Brandes and Ikeda (2004) capitalize on these strong and complementary polarimetric signatures in stratiform precipitation for freezing-level designation with accuracy to within 200 m. The Brandes and Ikeda (2004) technique matches observed polarimetric radar measurement profiles with idealized model profiles of  $Z$ ,  $L_{DR}$ , and  $\rho_{HV}$  expected in the ML. Tabary et al. (2006) present a similar technique for operational ML identification capitalizing solely on profiles of  $\rho_{HV}$ .

ML designation is an integral part of product generation for the polarimetric prototype of the Weather Surveillance Radar-1988 Doppler (WSR-88D). A fuzzy logic approach has been adopted for the operational

---

*Corresponding author address:* Alexander V. Ryzhkov, CIMMS/NSSL, 120 David L. Boren Blvd., Norman, OK 73072.  
E-mail: alexander.ryzhkov@noaa.gov

hydrometeor classification algorithm (HCA). The Joint Polarization Experiment (JPOLE) validated the performance of this approach for discrimination of non-meteorological echoes and the designation of hail (Ryzhkov et al. 2005b). However, the membership functions for several classes such as light rain and dry aggregate snow are significantly overlapped because of small polarimetric contrasts between these media. Accurate ML designation is crucial for successful delineation of these hydrometeors. QPE for the polarimetric WSR-88D may also be contingent on reliable radar echo classification such that different rainfall relations are utilized for different classes of hydrometeors in the radar resolution volume.

This paper presents an algorithm for operational polarimetric ML detection (MLDA). The technique differs from the Brandes and Ikeda (2004) and Tabary et al. (2006) methodology in that the algorithm does not attempt to match model profiles or rely on measurements of the linear depolarization ratio  $L_{DR}$ . The MLDA utilizes  $Z_{DR}$  instead of  $L_{DR}$  since a polarimetric prototype of the WSR-88D (KOUN herein) does not measure  $L_{DR}$  in its primary mode of operation for which horizontal (H) and vertical (V) waves are transmitted and received simultaneously (SHV mode). The proposed method designates an ML top and bottom rather than producing a single estimate of the freezing level height. The MLDA is integrated with the HCA in the operational system.

Verification of the proposed MLDA was performed for 18 events observed by the KOUN radar using 136 h of comparisons with Rapid Update Cycle (RUC) model output and National Weather Service (NWS) radio-sonde data when available.

## 2. Description of the MLDA

The proposed algorithm capitalizes on radial dependencies of  $Z$ ,  $Z_{DR}$ , and  $\rho_{HV}$  at elevation angles between  $4^\circ$  and  $10^\circ$  to estimate the boundaries of the ML. These radial dependencies reflect vertical profiles of the three radar variables that exhibit well-pronounced maxima in  $Z$  and  $Z_{DR}$  and minima in  $\rho_{HV}$ . The heights of these signatures generally do not coincide. Typically, the maximum of  $Z$  is observed at a higher altitude (i.e., at a larger slant range) than the maximum of  $Z_{DR}$  and minimum of  $\rho_{HV}$ . This can be explained by the fact that  $Z$  depends on concentration of melting snowflakes whereas  $Z_{DR}$  and  $\rho_{HV}$  measurements do not. Indeed, the vertical profile of  $Z$  within the melting layer is determined by three factors: 1) a change in particle size, 2) a change in particle refractive index, and 3) a change in particle concentration. As melting snowflakes fall

through the melting layer, their size may initially increase due to possible aggregation and eventually decreases when a snowflake melts into a water drop. Concurrently, refractive index monotonically increases while concentration decreases as a result of a rapid increase in terminal velocity. Since  $Z_{DR}$  does not depend on concentration, the decrease in concentration does not offset the increase in  $Z_{DR}$  due to possible aggregation and wetting of snowflakes. Hence, the maximum of  $Z_{DR}$  is observed closer to the bottom of the melting layer than the  $Z$  maximum. Similar considerations can be applied to  $\rho_{HV}$ .

Examples of ML signatures at an elevation of  $4.5^\circ$  are presented for a PPI and for a mean radial profile from the 13 May 2005 event in Figs. 1 and 2. These examples confirm that the  $\rho_{HV}$  signature provides the most effective discrimination of melting hydrometeors.

### a. Input radar data

For the WSR-88D precipitation volume coverage pattern (VCP-11), the MLDA incorporates six elevation angles:  $4.5^\circ$ ,  $5.5^\circ$ ,  $6.5^\circ$ ,  $7.5^\circ$ ,  $8.7^\circ$ , and  $10.0^\circ$ . Such a choice of elevation angles is dictated by a compromise between radar resolution and areal coverage for observing melting signatures. At elevation angles lower than  $4^\circ$ , ML signatures are smeared due to beam broadening and may be contaminated by nonuniform beam filling (NBF) or partial beam blockage (e.g., Sánchez-Diezma et al. 2000; Ryzhkov 2007; Giangrande and Ryzhkov 2005). The widening of ML signatures at grazing angles due to beam broadening may be even more significant for polarimetric measurements (e.g., Ryzhkov 2007). The impact of beam broadening is discussed in further detail in section 2d. At elevation angles greater than  $10^\circ$ , the expected number of range gates that reside within a typical ML decreases rapidly. In addition, at higher elevation angles, the ML signature is expected at closer slant ranges, which are more likely contaminated with ground clutter.

Ground clutter and nonmeteorological scatterers such as birds and insects may exhibit signatures similar to melting hydrometeors in the fields of  $Z$ ,  $Z_{DR}$ , and  $\rho_{HV}$ . Therefore, the results of radar echo classification obtained with the HCA are used to minimize spurious designations from nonmeteorological media. Doppler clutter filtering (not currently performed on KOUN) will also mitigate spurious designations associated with precipitation mixed with nonmeteorological echo.

### b. Identification of melting snow

The MLDA searches for gate locations exhibiting polarimetric signatures of melting snow. Identification is

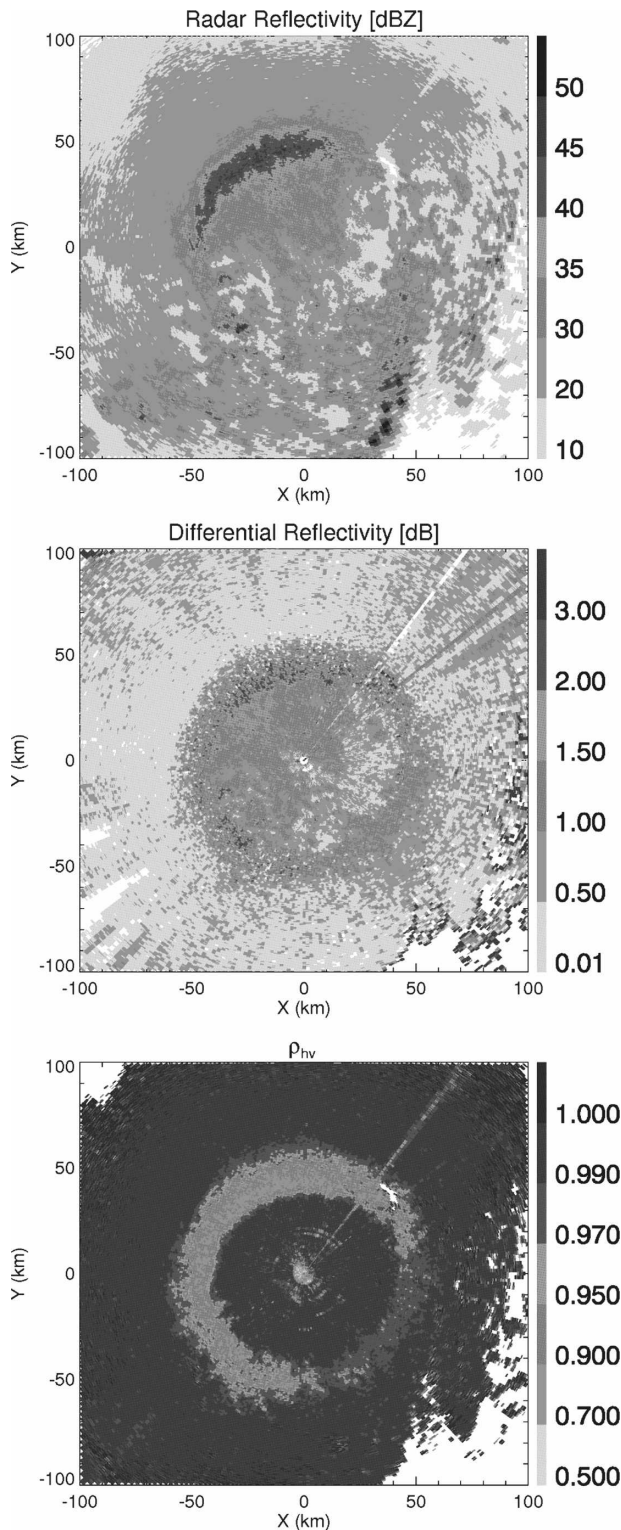


FIG. 1. KOUN measurement PPI images of  $Z$ ,  $Z_{DR}$ , and  $\rho_{HV}$  on 13 May 2005 at a  $4.5^\circ$  elevation angle.

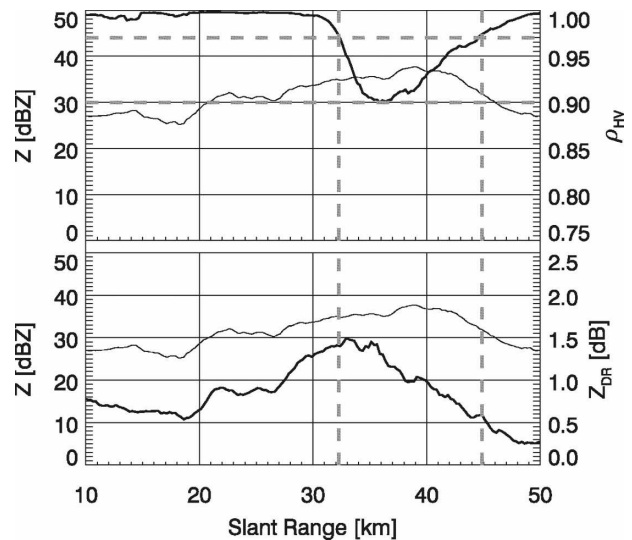


FIG. 2. An example of average slant range dependences of  $Z$ ,  $Z_{DR}$ , and  $\rho_{HV}$  at a  $4.5^\circ$  elevation angle for the case illustrated in Fig. 1;  $Z$  measurements are displayed with thin solid lines, and  $Z_{DR}$  and  $\rho_{HV}$  are displayed with thick solid lines. MLDA  $\rho_{HV}$  thresholds are depicted with dashed lines.

performed on preprocessed radial data. Data preprocessing for the KOUN radar includes a radial smoothing procedure using a three-gate averaging window for  $Z$  (0.5 km) and a five-gate window for  $Z_{DR}$  and  $\rho_{HV}$  (1.0 km). Here  $Z$  and  $Z_{DR}$  measurements are corrected for attenuation–differential attenuation in rain using differential phase along the radial. Additional KOUN processing details are available in Ryzhkov et al. (2005b). Identification of melting snow is performed as follows:

- 1) For each radial, we identify gates where  $\rho_{HV}$  falls between 0.90 and 0.97. These gates may not necessarily belong to the ML. Ground clutter and biological scatterers may exhibit similar  $\rho_{HV}$  signatures. To mitigate contamination from scatterers other than melting snowflakes, locations with polarimetric signatures of nonmeteorological echo are filtered. A climatological ML height constraint is enforced to ensure melting snowflakes are not identified above 6 km (adaptable threshold).
- 2) The  $\rho_{HV}$  ML signature should be consistent with  $Z$  and  $Z_{DR}$  maxima in the vicinity of the gate where the  $\rho_{HV}$  drop occurs. The algorithm searches for  $Z$  and  $Z_{DR}$  maxima in a 500-m window above gate locations matching the  $\rho_{HV}$  signature from step 1. The equivalent slant range distance for this window varies with elevation angle.
- 3) If the maximum value of  $Z$  falls between 30 and 47 dBZ and the maximum value of  $Z_{DR}$  is within the interval 0.8 to 2.5 dB for the 500-m window, then the gate of the  $\rho_{HV}$  signature is considered an ML point.

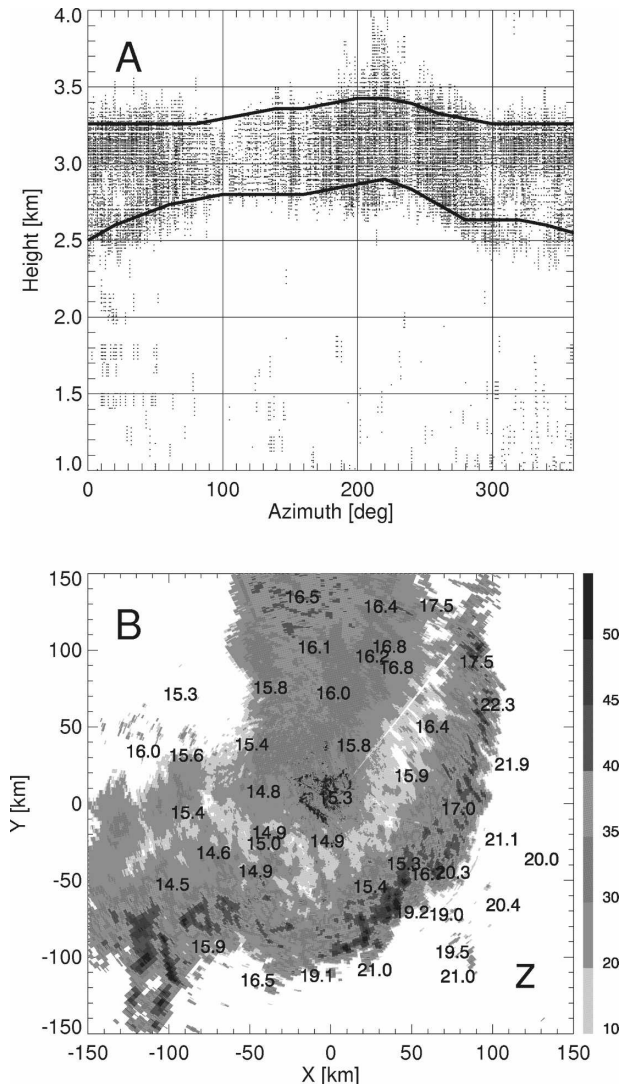


FIG. 3. (a) Example of ML points mapped on the height–azimuth plane. The 80% (ML top) and 20% (ML bottom) height contours are overlaid on the image in solid lines. (b) Corresponding surface Oklahoma Mesonet temperature ( $^{\circ}\text{C}$ ; plotted points) and KOUN radar reflectivity factor (gray shades) from a  $0.5^{\circ}$  elevation angle. Highest surface temperatures and higher ML tops are located in directions ahead of the convective line.

- 4) The corresponding azimuth and height of the ML points are stored in a two-dimensional array that contains the total number of ML points in a height–azimuth grid. The proposed MLDA utilizes a grid resolution of 0.1 km in height and  $1^{\circ}$  resolution in azimuth for this array. Figure 3 provides an example of the ML point locations on a height–azimuth plane after all azimuths and elevations between  $4^{\circ}$  and  $10^{\circ}$  are examined for a single radar volume (13 May 2005 event from the dataset, 0848 UTC).
- 5) ML signatures at higher elevations are less smeared by the radar beam and thus better pronounced. The

total number of possible ML points is smaller at higher elevations. In light of this, the MLDA can be modified to weight data collected at higher elevation angles more than the data collected at lower elevation angles.

- 6) Although censoring of ground clutter at lower heights is performed for regions with nonmeteorological polarimetric signatures, we found it useful to further mitigate possible contamination from ground clutter by removing ML points detected more than 1 km below the ML bottom height of the previous scan.

### c. Designation of the melting layer boundaries

Designation of ML boundaries is performed if the total count of ML points in the array exceeds a predetermined threshold (currently 1500 ML points). Typically, a high threshold produces more accurate results, but requires a longer time for data accumulation. ML boundaries are determined using the following methodology:

- 1) To capture azimuthal variability of the ML boundaries, the height–azimuth array of ML points is partitioned using a running (boxcar)  $21^{\circ}$  sector window ( $\pm 10^{\circ}$  around the azimuth of MLDA designation). If the total number of ML points in a sector exceeds an adaptable threshold, then ML designation will be performed for that particular sector. If not, designation is not possible for this sector.
- 2) The heights that encompass a majority of the ML points are determined. In the proposed algorithm, the ML top is determined as the height below which 80% of ML points reside. Similarly, the ML bottom is determined as the height below which 20% of the ML points reside. Example ML boundaries are presented with solid lines in Fig. 3.
- 3) Missing designations (e.g., directions not meeting the threshold requirements) are filled using valid ML radar retrievals. For example, if only a single sector qualifies for a valid designation, that designation is utilized for all azimuths.

### d. Justification of the thresholds in the MLDA procedure

The  $\rho_{\text{HV}}$  thresholds serve as the primary criteria for ML point identification along a radial. The lower MLDA  $\rho_{\text{HV}}$  threshold of 0.90 mitigates contamination from nonmeteorological scatterers. The upper  $\rho_{\text{HV}}$  threshold was selected to ensure the best discrimination between wet snow (within the melting layer) and light-to-moderate rain (below the melting layer) or dry snow (above the melting layer). The separation between

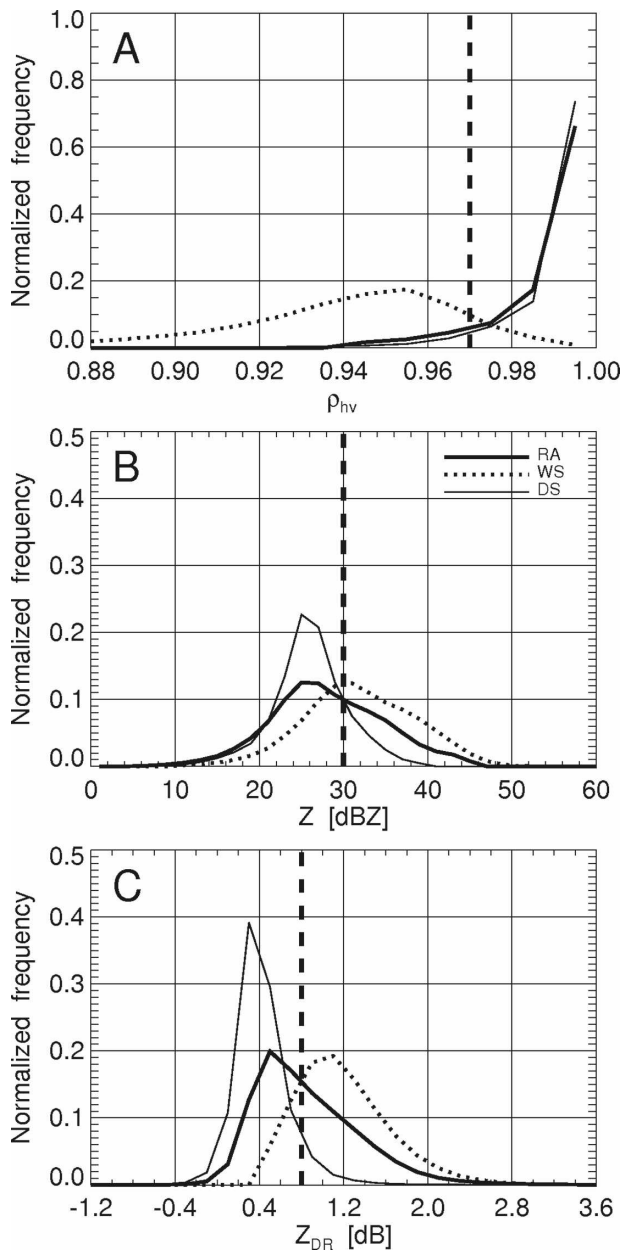


FIG. 4. Normalized histograms of KOUN radar measurements of (a)  $\rho_{HV}$ , (b)  $Z$ , and (c)  $Z_{DR}$  for wet snow (dotted line), dry snow (thin solid line), and light-to-moderate rain [thick solid line; adapted from Park et al. (2007), 29 h of observation]. Vertical dashed lines indicate thresholds used in the MLDA.

these three categories of hydrometeors in terms of  $\rho_{HV}$ , as well as  $Z$  and  $Z_{DR}$  is illustrated in Fig. 4. The histograms in Fig. 4 summarize the results of polarimetric hydrometeor classification for a large set of the KOUN data including 29 h of observations for six storm events in central Oklahoma (Park et al. 2007). Figure 4a presents normalized histograms of  $\rho_{HV}$  for the two types of snow and rain. It is evident from Fig. 4a that the best

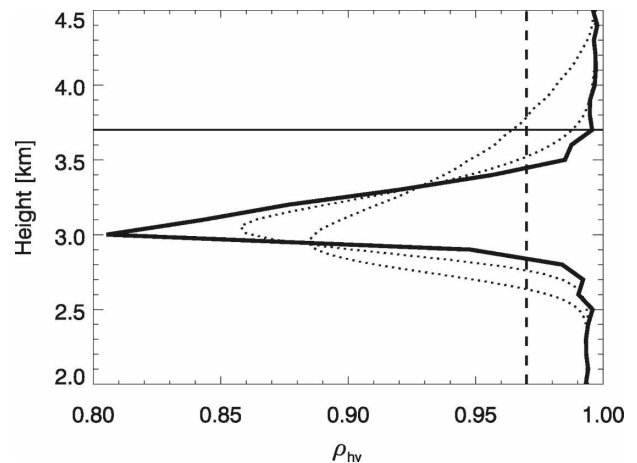


FIG. 5. Intrinsic model (thick solid line) and smoothed (dotted lines) vertical profiles of  $\rho_{HV}$  demonstrating the impacts of beam broadening and radial smoothing on polarimetric melting layer signatures at elevation angles of  $4.5^\circ$  and  $10.0^\circ$ . Environmental melting level height is approximately 3.7 km (thin horizontal line). The dashed vertical line shows the MLDA threshold of 0.97.

separation of wet snow (ML) from dry snow and rain is achieved if the demarcation value of  $\rho_{HV} = 0.974$  is used. This value is very close to the upper  $\rho_{HV} = 0.97$  threshold. The  $Z$  and  $Z_{DR}$  histograms for the three classes in Figs. 4b,c also substantiate the choice of the relevant  $Z$  and  $Z_{DR}$  thresholds in the MLDA.

We also consider the impact of radial smoothing and antenna beam broadening on the vertical profile of  $\rho_{HV}$  in justification of the  $\rho_{HV}$  thresholds. To evaluate such an impact, we take a model profile of intrinsic  $\rho_{HV}$  (solid line in Fig. 5) and compute the corresponding profiles modified by radial smoothing and beam broadening for elevation angles of  $4.5^\circ$  and  $10^\circ$  (dotted lines in Fig. 5) following the methodology suggested by Ryzhkov (2007). The shape of the model profile was obtained from KOUN measurements at very high elevation angles (between  $10^\circ$  and  $45^\circ$ ) without any radial smoothing for the case on 7 April 2002 (see Ryzhkov et al. 2005a). The height of the melting level (3.7 km) is adjusted to be more consistent with an average climatological value for central Oklahoma.

Although the model  $\rho_{HV}$  profile is almost symmetric, there is more broadening on the upper side because of very different vertical gradients of radar reflectivity factor above and below the melting layer. As expected, the broadening is more significant at an elevation of  $4.5^\circ$ . If the vertical profile of  $\rho_{HV}$  is not widened at all, then using the MLDA threshold of 0.97 (dashed vertical line) would result in about 0.25-km underestimation of the melting level height. Beam broadening and radial smoothing at elevations of  $10^\circ$  and  $4.5^\circ$  for this example causes about 0.1 km of underestimation and overesti-

mation of the freezing level height, respectively. Hence, at least a fraction of the ML points from a typical melting layer are expected at heights above the melting level. If all ML points are counted, overestimation of the melting level height is inevitable. This is one of the reasons for discarding ML points above the 80th percentile for estimation of the ML top.

The choice of the cutoff percentiles in the height distribution of ML points is quite subjective. Apparently, retaining too many ML points in the distribution tails leads to increasing statistical errors in determination of the ML top and bottom. On the other hand, decreasing the interval between the two cutoff percentiles too much would produce an artificially narrow melting layer (however, mitigating the impacts of beam broadening and radial smoothing). We believe that 20% and 80% is a reasonable compromise. Ultimately, an empirical correction is likely needed for any choice of the cutoff percentiles (see section 3).

#### *e. Additional considerations*

In addition to the use of multiple elevation angles to improve ML designation, the MLDA procedure retains information from previous volume scans to alleviate sparse data intervals in time and space and improve time continuity of the designation. This is accomplished by combining arrays of ML points corresponding to the current and two previous radar volume scans. With update times of 5 min, this translates to approximately a 15-min averaging window. From operational testing, the 15-min window reflects the shortest time-averaging interval that consistently produces spatially continuous ML boundaries. Previous studies by Gourley and Calvert (2003) indicate success with the use of a 30-min window.

For some events, it is possible that no pronounced ML signatures exist, the lowest radar tilt in the MLDA may overshoot storms–ML signatures at distance greater than 60 km, or the ML signature may be embedded in ground clutter hindering proper interpretation with KOUN. Because the MLDA capitalizes on the polarimetric signatures of melting snowflakes and not those associated with melting graupel or hail, ML designation is not available in convective events with an absence of surrounding regions of melting snow. For situations where an ML cannot be determined, model output temperatures, radiosonde and surface temperature data, or user-defined values are necessary to supplement the operational products or until sufficient radar melting signatures can be accumulated. Such considerations allow for uninterrupted application of ML designation for a generation of other polarimetric radar products.

### **3. Validation of melting layer designation**

First, we would like to make a distinction between the melting layer and melting level. Following the *Glossary of Meteorology* (Glickman 2000), the melting layer is defined as the altitude interval throughout which ice-phase precipitation melts as it descends. The melting level is defined as the lowest 0°C constant temperature surface and the top of the melting layer. In stratiform and widespread precipitation events, it is expected that the retrieved ML top should coincide well with the location of the melting level since the onset of snowflake melting is typically at temperatures of 0°C or slightly warmer. The height of the ML bottom is variable and may be several hundred meters below the melting level at temperatures warmer than 5°C depending on humidity, particle concentration, or density (e.g., Stewart et al. 1984; Pruppacher and Klett 1997; Willis and Heymsfield 1989; Fabry and Zawadzki 1995). The thickness of the ML has been observed close to 500 m according to long-term ML observations (e.g., Fabry and Zawadzki 1995).

The performance of the MLDA has been tested for several precipitation events in central Oklahoma. A list of the 18 events and the validation sources for these events is provided in Table 1. Designations of the top and bottom of the ML have been checked against high-frequency RUC model analysis output (e.g., Benjamin et al. 2004). ML top designations have also been validated against radiosonde observations. Areal averaged ML top heights (average ML top-height designation from all valid azimuthal directions) retrieved from the KOUN radar are compared to the heights of the lowest 0°C level from these sources. Radiosonde data are obtained from the Norman, Oklahoma (OUN), NWS radiosonde site that is within 200 m of the KOUN radar site. RUC model analysis output from the closest model grid points is interpolated over the KOUN radar location.

#### *a. Comparison with radiosonde observations*

Radiosonde temperature and height measurements from the NWS Norman (OUN) location are available at 0000 and 1200 UTC (Vaisala RS80 radiosonde equipment). The nearest valid radar-based designation (to within an hour and a half of the OUN sounding) is utilized for comparisons. Because of the limited sounding frequency, radiosonde-derived 0°C levels in close temporal proximity are not available for all events listed in Table 1. The Thunderstorm Electrification and Lightning Experiment (TELEX) field campaign high-resolution Multi-Channel Atmospheric Sounding System (MCASS) balloon launch data supplement OUN

TABLE 1. KOUN data listing and available verification for melting layer designation.

Event	ML designation	RUC hours	Radiosonde source	Sonde hour
21 May 2003	1236–1437 UTC	1200–1500 UTC	NWS Norman, OK	1200 UTC
4 Jun 2003	1204–1839 UTC	1200–1900 UTC	NWS Norman, OK	1200 UTC
11 Jun 2003	0056–0601 UTC	0100–0600 UTC	NWS Norman, OK	0000 UTC
2 Jun 2004	2117–2210 UTC	2100–2200 UTC	—	—
3 Jun 2004	0201–0559 UTC	0200–0600 UTC	—	—
9 Jun 2004	0714–2359 UTC	0700–2300 UTC	NWS Norman, OK	1200 UTC 0000 UTC
19 Jun 2004	1155–1837 UTC	1100–1900 UTC	NWS Norman, OK	1200 UTC
20 Jun 2004	1628–1753 UTC	1600–1800 UTC	TELEX MCASS	1648 UTC
21 Jun 2004	0936–1658 UTC	0900–1700 UTC	NWS Norman, OK	1200 UTC
22 Jun 2004	0503–1410 UTC	0500–1200 UTC	NWS Norman, OK	1200 UTC
14 Nov 2004	1917–2359 UTC	1900–2300 UTC	NWS Norman, OK	0000 UTC
15 Nov 2004	0643–2025 UTC	0700–2000 UTC	NWS Norman, OK	1200 UTC
18 Nov 2004	0029–0337 UTC	0000–0400 UTC	NWS Norman, OK	0000 UTC
	0553–0559 UTC	0600 UTC		
6 Feb 2005	0122–1455 UTC	0100–1500 UTC	NWS Norman, OK	1200 UTC
13 May 2005	0657–1253 UTC	0700–1300 UTC	NWS Norman, OK	1200 UTC
4 Jun 2005	2222–2359 UTC	2200–2300 UTC	NWS Norman, OK	0000 UTC
5 Jun 2005	0000–0259 UTC	0000–0300 UTC		
13 Jun 2005	0112–0322 UTC	0100–0300 UTC	NWS Norman, OK	0000 UTC
	2140–2305 UTC	2200–2300 UTC		
17 Jun 2005	0403–0501 UTC	0400–0500 UTC	—	—

soundings for select events during summer 2004 (as noted in Table 1).

Areal averaged ML top heights from the MLDA are plotted against the radiosonde-derived melting level heights in Fig. 6. The plot contains all available hours of comparison (16 h total). The bias of the radar estimate for this dataset is  $-0.18$  km with an RMS error of 0.28 km and standard deviation of 0.21 km. The correlation between ML top obtained from the radar and radiosonde-derived  $0^{\circ}\text{C}$  height is 0.92.

#### b. Comparison with RUC model analysis output

Operational forecast models may provide accurate estimates of the melting level height to within a few hundred meters, particularly in uniform precipitation events (e.g., Mittermaier and Illingworth 2003). An advantage of the RUC model is the high spatial and temporal resolution of its output. Hence, longer series of continuous radar-based ML designations can be validated.

A comparison of areal averaged ML top height and RUC model analysis output  $0^{\circ}\text{C}$  height is presented in Fig. 7. The plot contains 136 h of RUC-radar comparisons for the 18 events in Table 1. Although the majority of points in Fig. 7 group very well along the  $45^{\circ}$  line, there is a separate cluster of points denoted with asterisks for which the radar shows a substantially lower height of the melting level relative to the RUC model. These points are associated with a few warm-season

convective events for which the RUC output may not be a reliable verification source. We will discuss this issue in more detail in the next section. After these spurious hours are removed, a subset of 115 h remains. For this subset, the bias is  $-0.16$  km with an rms error

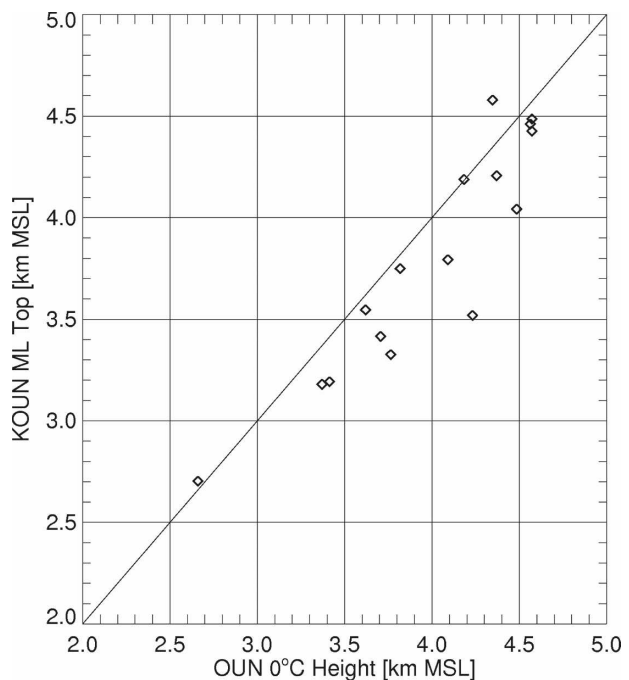


FIG. 6. Scatterplot of ML top heights obtained from the MLDA vs radiosonde-derived  $0^{\circ}\text{C}$  observations.

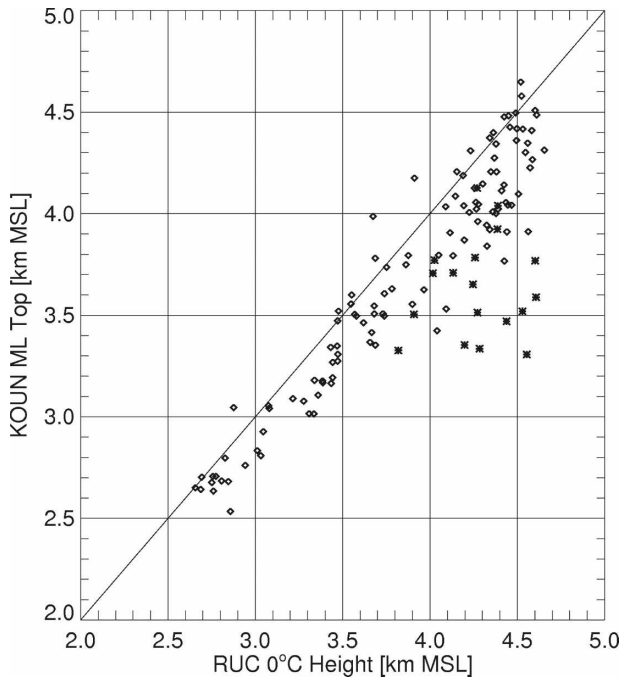


FIG. 7. As in Fig. 6, but utilizing RUC model analysis output temperatures for validation. Hours with questionable RUC or MLDA performance for convective events are noted with asterisks.

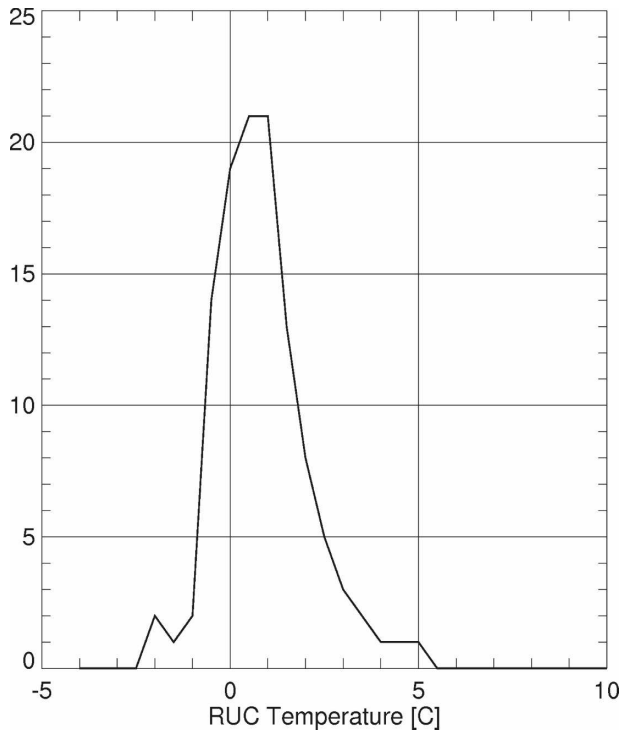


FIG. 8. Histogram of the temperature of the ML top retrieved from the radar as revealed by RUC model analysis output.

of 0.27 km and standard deviation of 0.22 km. The correlation between ML top heights and RUC model-derived melting level height is 0.93.

Figure 8 displays a histogram of the RUC model temperature associated with the heights of the ML top designations for the hours of available RUC model output. The histogram is plotted at 0.5°C temperature bin intervals. Similar analysis was performed for ML bottom designations in Fig. 9. ML bottom designation indicates a wider range of associated temperatures, with the ML bottom often identified between RUC 2° and 6°C. Events with extremely warm ML bottom designations (e.g., RUC temperature greater than 5°C) are typically associated with mature warm-season convective line events featuring trailing precipitation regions and/or questionable RUC or ML retrieval performance. A histogram of MLDA ML depth (ML top minus ML bottom) for the hours of the RUC model dataset is presented in Fig. 10. ML thickness is typically less than 500 m, consistent with long-term ML thickness observations by Fabry and Zawadzki (1995).

*c. Temporal dependencies*

Checking temporal and spatial continuity of ML retrievals is a simple test of the algorithm performance. Since the radar ML designations in our dataset were

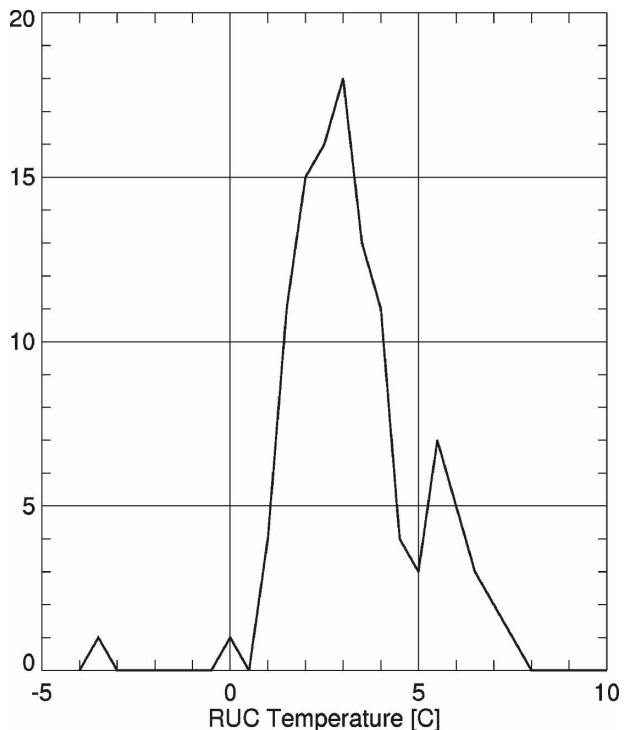


FIG. 9. As in Fig. 8, but for ML bottom heights.

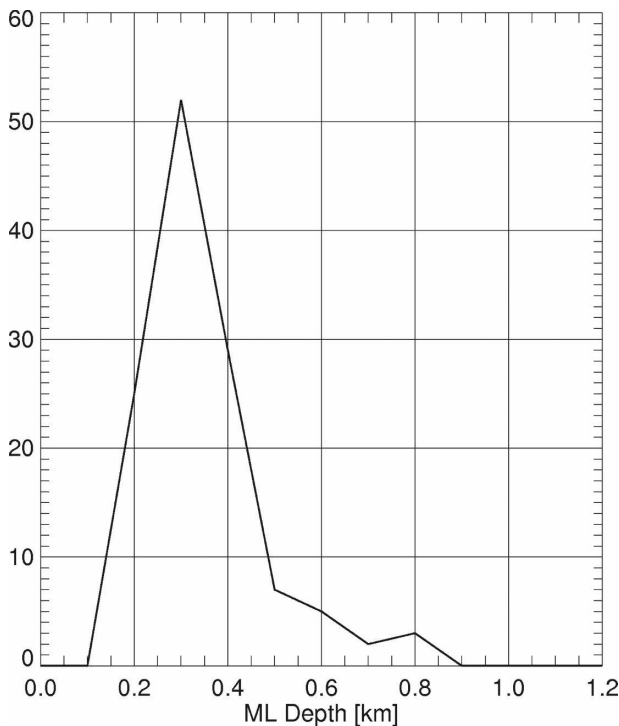


FIG. 10. Histogram of the ML thickness retrieved from the MLDA.

updated every 5 min for the periods of several hours, it was possible to trace general trends and sharp changes in the characteristics of air masses associated with frontal passage or convective lines (Fig. 11). Temporal dependencies of areal averaged ML top heights are provided in Fig. 11 for four long-duration events in the dataset. Crosshairs on the image indicate results of the radar retrieval. NWS radiosonde-derived melting level heights are denoted with an “S” symbol. Melting level heights obtained from the RUC are shown with diamonds. Error bars for the radar estimates reflect the degree of azimuthal variability.

#### 4. Discussion

Overall, areal averaged height of the melting level (ML top) estimated from the MLDA correlates very well (at the level of 0.92–0.93) with heights obtained from soundings or RUC model analysis output except for a few outliers typically associated with mature warm-season MCSs. If the outliers are excluded, then the radar algorithm yields a negative bias between 0.16 and 0.18 km. Most bias is attributed to the cutoff percentile choice of 80% for the ML top. One may reduce or eliminate most bias if a higher percentile threshold is chosen. However, an increase of this threshold may re-

sult in noisier retrievals. Thus, we prefer to use the 80th percentile level for the ML top designation and add an empirically derived correction of 0.16 km. This would ensure the unbiased estimate and the rms error of 0.22 km. An offset (although perhaps less pronounced) is expected for ML bottom retrievals; however, limited observations are available to validate this offset.

Several additional factors may also contribute to a discrepancy between the areal averaged estimates of the ML heights from radar, soundings, and model analysis output. One of them is azimuthal variability of the ML height that is not captured by spatially sparse NWS soundings and quite often is not well reproduced in RUC model output. In the case of widespread radar echo typical for large frontal systems or trailing stratiform regions of MCS events, the polarimetric radar demonstrates a unique capability to track spatial variations in the depth and height of the ML including small-scale undulations of the melting level (e.g., due to localized convection or the passage of convective lines, as highlighted in the lower panel of Fig. 3). As error bars in Fig. 11 indicate, spatial variability of the MLDA-retrieved height exceeds 300 m for several events. The radar provides ML retrievals only in the areas of radar echo, whereas many soundings used for validation were collected in precipitation free air.

MLDA update frequency can provide a significant improvement over RUC model analysis output, which is available hourly with observational data assimilation “cutoff” times that may delay the analysis output by 20–50 min after the analysis time. RUC model analyses rely on the previous 1-h forecast, which may exhibit errors, particularly in convective regimes. A benefit of high-resolution radar ML retrieval is well illustrated with an example of the 13 May 2005 event (Fig. 11d) featuring an intense convective line and trailing precipitation region in the vicinity of the KOUN radar location. As the system approaches the radar location, the RUC 0°C height and radar areal averaged ML heights significantly differ. By 1200 UTC, the RUC 0°C height and the overall temperature profile change markedly following the RUC assimilation of the 1200 UTC OUN sounding. The change is indicative of prior questionable performance of the RUC model for this event. For the 1200 UTC analysis time, the MLDA top height is in best agreement with RUC model 0°C height and the OUN sounding. It is noted that the 1200 UTC OUN sounding was most likely launched into a relatively precipitation-free environment behind the trailing stratiform region, which may account for the observed mismatch of about 400 m between the OUN and MLDA designations.

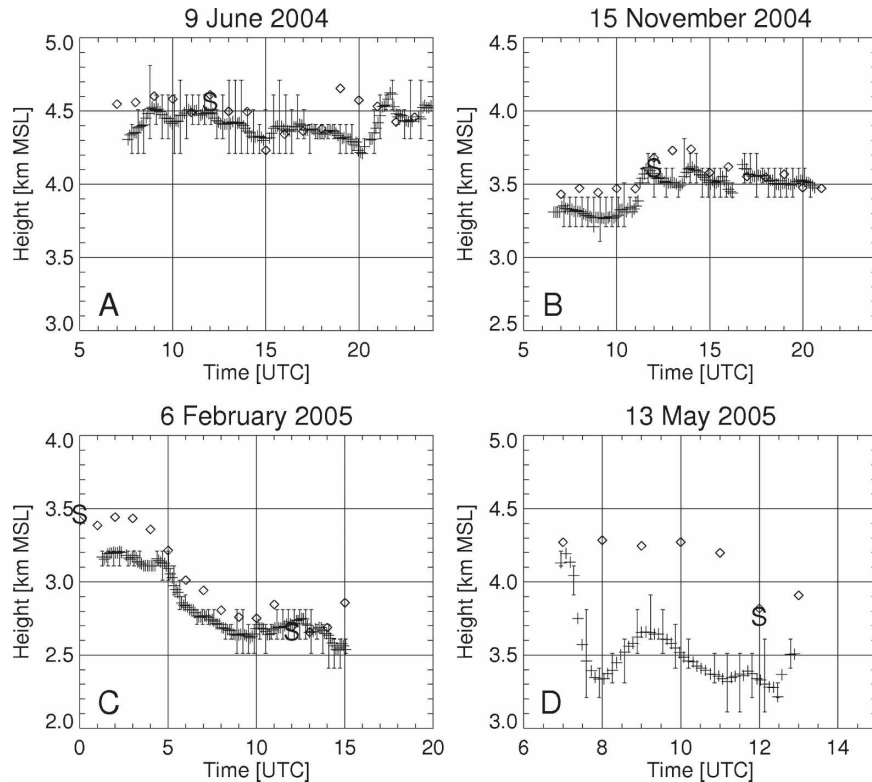


FIG. 11. Temporal dependencies of the height of the ML top estimated from the radar (crosses), RUC model output (diamonds), and soundings (“S” symbol, bottom of the symbol) for 4 different days of observation.

## 5. Summary

- 1) A new melting layer detection algorithm (MLDA) has been developed for use with the polarimetric WSR-88D. The algorithm estimates the top and bottom boundaries of the ML using radar reflectivity factor  $Z$ , differential reflectivity  $Z_{DR}$ , and cross-correlation coefficient  $\rho_{HV}$  measured at antenna elevations between  $4^\circ$  and  $10^\circ$ .
- 2) The suggested algorithm was validated using sounding data and the output of the RUC model for 18 events encompassing 136 h of observations in central Oklahoma. The height of the top of the ML retrieved from the radar was compared with the height of the lowest  $0^\circ\text{C}$  isotherm obtained from soundings and the RUC model.
- 3) In 85% of cases, the MLDA yields unbiased estimates of the height of the melting level with an RMS error of 0.22 km. The correlation coefficient between the radar estimates and the ones from soundings and the RUC model output was as high as 0.92 and 0.93, respectively, for this category of events (mainly widespread stratiform rain).
- 4) The remaining 15% of the cases were primarily as-

sociated with mature warm-season mesoscale convective systems for which radar-derived ML heights were occasionally 1 km lower than the RUC model prediction. There is a strong indication that the radar might provide more reliable designation of the ML than the RUC model in these situations.

- 5) It was found that the temperature of the bottom of the ML varies in a wide range from  $2^\circ$  to  $6^\circ\text{C}$ . According to MLDA retrievals, the depth of the ML changed from 100 to 900 m with a median value of about 400 m in the dataset used for validation.
- 6) The MLDA product updated every 5 min exhibiting solid temporal continuity and consistency with model output and soundings.
- 7) It is demonstrated that the MLDA captures the azimuthal and spatial variability of the height of the ML in the cases of widespread precipitation.
- 8) The MLDA is considered as an essential part of the operational polarimetric radar echo classifier to be used with polarimetrically upgraded WSR-88Ds.

*Acknowledgments.* The authors thank Dan Suppes for his support in the generation of data for this paper.

We thank J. J. Gourley (NSSL) and T. Schuur (NSSL) for review of the manuscript. RUC model analysis output and support was provided by M. Baldwin (Purdue University, formerly NSSL) and K. Manross (NSSL). The authors also thank the principal TELEX field campaign investigators and support staff for the balloon sounding for the 20 June 2004 event. Funding was provided by NOAA/Office of Oceanic and Atmospheric Research under NOAA–University of Oklahoma Cooperative Agreement NA17RJ1227, U.S. Department of Commerce. Part of this work was supported by the National Weather Service, the Federal Aviation Administration, and the NEXRAD Product Improvement Program.

#### REFERENCES

- Benjamin, S. G., and Coauthors, 2004: An hourly assimilation–forecast cycle: The RUC. *Mon. Wea. Rev.*, **132**, 495–518.
- Brandes, E. A., and K. Ikeda, 2004: Freezing-level estimation with polarimetric radar. *J. Appl. Meteor.*, **43**, 1541–1553.
- Fabry, F., and I. Zawadzki, 1995: Long-term radar observations of the melting layer of precipitation and their interpretation. *J. Atmos. Sci.*, **52**, 838–851.
- Giangrande, S. E., and A. V. Ryzhkov, 2005: Calibration of dual-polarization radar in the presence of partial beam blockage. *J. Atmos. Oceanic Technol.*, **22**, 1156–1166.
- Glickman, T., Ed., 2000: *Glossary of Meteorology*. 2nd ed. Amer. Meteor. Soc., 855 pp.
- Gourley, J. J., and C. M. Calvert, 2003: Automated detection of the bright band using WSR-88D data. *Wea. Forecasting*, **18**, 585–599.
- Mittermaier, M. P., and A. J. Illingworth, 2003: Comparison of model-derived and radar-observed freezing-level heights: Implications for vertical reflectivity profile-correction schemes. *Quart. J. Roy. Meteor. Soc.*, **129**, 83–95.
- Park, H.-S., A. V. Ryzhkov, D. S. Zrnic, and K.-E. Kim, 2007: Optimization of the matrix of weights in the polarimetric algorithm for classification of radar echoes. Preprints, *33rd Conf. on Radar Meteorology*, Cairns, Australia, Amer. Meteor. Soc., P11B.4. [Available online at <http://ams.confex.com/ams/pdfpapers/123123.pdf>.]
- Pruppacher, H. R., and J. D. Klett, 1997: *Microphysics of Clouds and Precipitation*. 2nd ed. Kluwer Academic, 954 pp.
- Ryzhkov, A. V., 2007: The impact of beam broadening on the quality of radar polarimetric data. *J. Atmos. Oceanic Technol.*, **24**, 729–744.
- , S. E. Giangrande, V. M. Melnikov, and T. J. Schuur, 2005a: Calibration issues of dual-polarization radar measurements. *J. Atmos. Oceanic Technol.*, **22**, 1138–1155.
- , T. J. Schuur, D. W. Burgess, P. L. Heinselman, S. E. Giangrande, and D. S. Zrnic, 2005b: The Joint Polarization Experiment: Polarimetric rainfall measurements and hydrometeor classification. *Bull. Amer. Meteor. Soc.*, **86**, 809–824.
- Sánchez-Diezma, R., I. Zawadzki, and D. Sempere-Torres, 2000: Identification of the bright band through the analysis of volumetric radar data. *J. Geophys. Res.*, **105**, 2225–2236.
- Stewart, R. E., J. D. Marwitz, J. C. Pace, and R. E. Carbone, 1984: Characteristics through the melting layer of stratiform clouds. *J. Atmos. Sci.*, **41**, 3227–3237.
- Tabary, P., A. Le Henaff, G. Vulpiani, J. Parent-du-Châtelet, and J. J. Gourley, 2006: Melting layer characterization and identification with a C-band dual-polarization radar: A long-term analysis. Preprints, *Fourth European Conf. on Radar in Meteorology and Hydrology (ERAD 2006)*, Barcelona, Spain, Servei Meteorologic de Catalunya, 17–20.
- Willis, P. T., and A. J. Heymsfield, 1989: Structure of the melting layer in mesoscale convective system stratiform precipitation. *J. Atmos. Sci.*, **46**, 2008–2025.
- Zrnić, D. S., N. Balakrishnan, C. L. Ziegler, V. N. Bringi, K. Aydin, and T. Matejka, 1993: Polarimetric signatures in the stratiform region of a mesoscale convective system. *J. Appl. Meteor.*, **32**, 678–693.